Microchim Acta (2017) 184:1059–1067
DOI 10.1007/s00604-017-2102-x

ORIGINAL PAPER

Fabrication of SERS active gold nanorods using benzalkonium chloride, and their application to an immunoassay for potato virus X

Mehmet Gokhan Caglayan[1] · Esin Kasap[2] · Demet Cetin[3] · Zekiye Suludere[4] · Ugur Tamer[2]

Received: 12 August 2016 / Accepted: 23 January 2017 / Published online: 4 February 2017

Abstract The authors report on a robust method for the synthesis of gold nanorods (AuNRs) with tunable dimensions and longitudinal surface plasmon resonance. The method relies on seed-mediated particle growth in the presence of benzalkonium chloride (BAC) in place of the widely used surfactant cetyltrimethyl ammonium bromide (CTAB). Uniform AuNRs were obtained by particle growth in solution, and BAC is found to stabilize the AuNRs for >1 year. The SERS activity of the resulting AuNRs is essentially identical to that of CTAB-protected nanorods. The SERS activity of the BAC protected nanorods was applied to the quantitative analysis of potato virus X (PVX). The calibration plot for PVX is linear in the 10 to 750 ng·mL^{-1} concentration range, and the detection limit is 2.2 ng·mL^{-1}.

Keywords Nanoparticles · Surfactant · Particle capping · Raman spectroscopy · Surface enhanced raman spectroscopy · Sandwich immunoassay · Magnetic nanoextraction

Electronic supplementary material The online version of this article (doi:10.1007/s00604-017-2102-x) contains supplementary material, which is available to authorized users.

✉ Ugur Tamer
utamer@gazi.edu.tr

[1] Department of Analytical Chemistry, Faculty of Pharmacy, Ankara University, 06100 Ankara, Turkey

[2] Department of Analytical Chemistry, Faculty of Pharmacy, Gazi University, Etiler, 06330 Ankara, Turkey

[3] Science Teaching Programme, Faculty of Education, Gazi University, Besevler, 06500 Ankara, Turkey

[4] Department of Biology, Faculty of Science, Gazi University, Besevler, 06500 Ankara, Turkey

Introduction

Chemical and physical behaviors of metal nanostructures are different from bulk materials because of quantum size effect resulting in specific electronic structures and these properties are dependent of their shape and size [1, 2]. The types and ratios of stabilizing agent, reducing agent and other chemicals determine these tunable properties in chemical synthesis of nanostructures. Among metal nanoparticles, gold nanoparticles have special interest and wide range of applications including biological applications like sensing, delivering and labeling [3–5]. Due to tunability of localized plasmon resonances of gold nanorods (AuNR), the synthesis of monodisperse novel AuNR is an appealing field of research [6–8]. Several methods were reported to synthesize AuNR with controllable size and aspect ratio utilizing seed – mediated growth [9]. Especially stabilizing agents that surrounds gold nanoparticles are essential in chemical and biological applications [4, 10]. One of the most used stabilizing agent in gold nanoparticle synthesis is cetyltrimethyl ammoniumbromide (CTAB) which yields stable gold nanoparticles [11]. In general, use of an acidic and weak reducing agent on a spherical gold nanoparticle (seed) in the presence of CTAB and silver ions leads AuNR formation with different aspect ratio. It is well documented that CTAB is a shape inducing agent and provides colloidal stability via shielding to prevent aggregation [12]. The exact mechanism involved in the anisotropic growth of gold nanorods in the seeded growth method is still lacking at a molecular level. However, silver plays important role during growth by formation of AgBr (bromide comes from CTAB) and getting deposited on 110 facet of gold surface. This promotes directed growth of gold nanorod from a facet which is less densely covered [13, 14]. Surfactant has also contribution to this unequal deposition on different facets. In this surfactant

contribution, known as a zipping mechanism, the van der Waals interactions between hydrophobic tails within the CTAB bilayer would favor the longitudinal growth of the nanorod [6, 10].

However, cytotoxicity of CTAB capped gold nanoparticles is a concern in biological applications because CTAB has acute toxicity in most human cells [15, 16]. In this study, we offer an alternative cationic surfactant in gold nanorod synthesis: benzalkonium chloride (BAC) which is cheaper and less toxic than CTAB. BAC has been frequently used as a preservative in drugs and disinfectant in various applications [17]. Especially in ophthalmic solutions, it is the most frequently used preservative because it efficiently fights microbial contamination in bottles and also permits antimicrobials and antihypertensives to enter the anterior chamber by breaking cell-cell junction in the corneal epithelium [18, 19]. In the AuNR synthesis, concentrated CTAB has ability to form elongated rod-like micellar structures [20] and BAC has also similar tendency to form rod-like micelles [21]. The reported zipping mechanism as proposed the longitudinal growth of AuNR would favor identical nanorod growth [22]. Like CTAB, BAC has quaternary ammonium group through which BAC might interact with gold surfaces. Long alkyl chain and a phenyl group connected to quaternary ammonium in BAC can help stabilization of colloids.

Surface Enhanced Raman Spectroscopy (SERS) has great potential in biological applications due to high sensitivity which is sufficient for detection of trace biomolecules in complex biological matrix or even single molecule detection [23]. Fabrication of novel gold nanostructures is also important in SERS since SERS amplification strongly depends on plasmons on the surface of gold nanoparticles [24]. Recent studies have explicitly demonstrated that gold nanoparticles possess different optical properties and localized surface plasmon resonance that is essential in SERS [25]. In particular, anisotropic nanoparticles, AuNR, have strong electromagnetic field enhancements due to sharp corners and SERS intensity of a molecule at these sites has substantially increased [26]. The contributions from both electromagnetic and chemical enhancement may promote stronger SERS activity of AuNR than that of spherical gold nanoparticles [27]. Furthermore, the probe molecules can be easily attached to the gold surface via the gold-thiolate bonding, [28] which is essentially identical to the strong covalent bonding. Novel gold particles as SERS substrates can be used to maximize signals for intended analytes and makes the ultra-sensitive analysis possible with a Raman spectrometer. However sensitivity is not only concern for the fabrication of a new nanomaterials in SERS if it is aimed to use them in a quantitative analysis, different issues from colloidal stability to reproducibility should be taken into account [23]. A major advance is demonstrated herein the growth of BAC capped gold nanorods (BAC-AuNR) was achieved using single – component surfactant system are essentially identical to CTAB capped gold nanorods (CTAB-AuNR). Replacement of CTAB by BAC surfactant during AuNR synthesis results in monodisperse AuNR formation with anisotropic optical properties. We also studied analytical performance of the synthesized particle in the quantitative analysis of potato virus X (PVX) by SERS. PVX is the type member of the genus *potexvirus* and it is one of the most useful model system studying different aspects of virus infections in plant virus research [29]. Surface modification efficiencies of CTAB-AuNR and BAC-AuNR by thiol replacement on the surfaces were also studied.

Material & method

Chemicals and instrumentation

N-Ethyl-*N*′-(3-dimethylaminopropyl)carbodiimide hydrochloride (EDC), N- Hydroxysuccinimide (NHS), ascorbic acid, NaOH, $HClO_4$, $FeSO_4$, $FeCl_3$, $AgNO_3$, $HAuCl_4$, phosphate buffered saline (PBS) tablets, ethanol, hydroxylamine hydrochloride, CTAB, 5,5′-Dithiobis(2-nitrobenzoic acid) (DTNB) were ordered from Sigma Aldrich (Germany, http://www.sigmaaldrich.com). Benzalkonium chloride solution (50%) was obtained from Tekkim (Bursa, Turkey, http://www.tekkim.com.tr). PVX and PVX antibody were purchased from Loewe Biochemica GmbH (Sauerlach, Germany, http://www.loewe-info.com). Water was ultrapurified by Mili-Q, Milipore system (18 MΩ cm).

Raman spectra were measured with DeltaNu Examiner Raman Microscopy system (Deltanu Inc., Laramie, WY, USA, https://www.sciaps.com) with a 785-nm laser source, a motorized microscope stage sample holder, and a cooled charge-coupled device (at 0 °C) detector. Instrument parameters were as follows: 150-mW laser power, 30-s acquisition time, 2-μm laser spot size and 20 × objective. UV-Vis spectra were measured by Agilent Technologies Cary 60 spectrophotometer (Santa Clara, CA, USA, http://www.agilent.com). Transmission electron microscopy (TEM) measurements were conducted with a JEOL TEM instrument (Peabody, MA, USA, http://www.jeolusa.com). Gold and sulfur amounts were measured with a THERMO ELECTRON X7 inductively coupled plasma-mass spectrometer (ICP-MS) (Waltham, MA USA, http://www.thermofisher.com). IR spectra were measured with Perkin Elmer Spectrum 400 FTIR/FTNIR (Waltham, MA USA, http://www.perkinelmer.com)

Seed-growth synthesis of gold nanoparticles

The procedure for AuNR synthesis started with seed formation reducing 250 μL $HAuCl_4$ (0.01 M) by freshly prepared ice cold 600 μL $NaBH_4$ (0.01 M) in the presence of 7.5 mL

CTAB in an ice bath. Then, 1.15 mL $HAuCl_4.3H_2O$ (0.01 M) was added to 4.75 mL of BAC (10%) to get orange growth solution in another vial. Then, 60 μL 0.01 M $AgNO_3$ and 250 μL 0.1 M ascorbic acid were added to the growth solution subsequently. The resulting solution was colorless. Finally, 100 μL seed solution was added on growth solution and gently shaken for 10 s. After three hours of waiting, blue colored solutions. Solutions were centrifuged for 10 min at 12,500 rpm (12,453 rcf) to remove excess BAC. After centrifugation, AuNR were suspended in deionized water or buffer depending upon the intended purposes.

Synthesis of iron oxide core gold Shell magnetic nanoparticle

Iron oxide core – gold shell magnetic nanoparticles (MGNP) was used for magnetic nano-extraction of PVX in SERS application of AuNR. For this aim, MGNP were prepared according to our previous procedure [30]. Briefly, iron oxide nanoparticles were formed by co-reduction of 5 mL $FeCl_3$ (1.28 M) and $FeSO_4$ (0.64 M) after dropwise addition of 1.0 M NaOH (125 mL). Iron oxide particles were collected by a magnet and washed with deionized water. Then they were kept in 2 M $HClO_4$ for 24 h and they were centrifuged at 10,000 rpm (8609 rcf) for 10 min. Iron oxide particles were dried at room temperature and 10 mg of them was dissolved in 5 mL water. Then 0.5 g ethylenediaminetetraacetic acid in 5 mL NaOH was added. After centrifugation at 8000 rpm (6887 rcf), 7 ml CTAB (0.1 M), 3 mL HAuCl4 (0.01 M), 0.35 mL NaOH (1 M), and 0.15 g hydroxylamine hydrochloride were added to iron oxide particles respectively. Wine-red color formation indicated surface covering of iron oxide particle with gold shell.

Characterization of nanoparticles

Nanoparticles were characterized according to their colors, UV-Vis absorption spectra and transmission electron microscope (TEM) images. UV-Vis absorption measurements of gold nanoparticles were measured between 400 and 800 nm. Gold nanoparticle samples were prepared on carbon/formvar coated copper grids and they were recorded on a TEM operated at 80 kV. Sulfur and gold amount in the nanoparticles after modification with some mercapto-compounds were measured with an ICP-MS. Silver content of the nanorod was also measured with the ICP-MS. Zeta potentials were measured for testing stability of AuNR. IR spectra were measured to observe BAC on the surface of AuNR.

Surface modification with mercapto-compounds

Surfaces of BAC-AuNR and CTAB-AuNR were modified with different mercapto-compounds; mercaptoundecanoic acid, lipoic acid and mercaptophenyl boronic acid: 1 mL BAC-AuNR and 1 mL CTAB-AuNR were centrifuged at 10000 rpm (14,000 rcf) for 10 min and washed with distilled water for three times separately. After three times washing, they were suspended in ethanolic solution of 20 mM 1 mL mercapto compounds separately and they were incubated for one night on a shaker. Then they were centrifuged and washed for three times with ethanol. After suspending in 5 mL water, finally Au and S amounts were measured with an ICP-MS.

SERS applications

Signal amplification of BAC-AuNR was firstly tested by using a Raman tag, DTNB. Signal enhancements by BAC-AuNR and CTAB-AuNR on DTNB were also compared. For this aim, same concentrations of AuNR were washed with water for three times after centrifugation at 1000 rpm for 10 min. Then they were suspended in ethanol containing 100 mM DTNB. After 1 h incubation at room temperature, AuNR were washed with ethanol for three times for removing excess DTNB and they were resuspended in ethanol. SERS spectra were obtained after evaporation of 3 μL samples on glass surface at room temperature. After signal enhancement study, BAC-AuNR was used for determination of PVX in a sandwich assay with MGNP. BAC-AuNR was modified with DTNB and PVX antibody for Raman labeling, while MGNP was modified with PVX-antibody for extraction.

BAC-AuNR solution was washed with water for three times after centrifugations at 1000 rpm for 10 min. They were suspended in ethanol and incubated for 1 h with a Raman label, DTNB (100 mM). After washing excess DTNB, carboxylate groups of DTNB were activated with EDC/NHS (0.1 M) for modification with PVX-antibody. Then they were incubated at 4 °C for one night with PVX-antibody. Excess PVX-antibody was washed with PBS for three times.

For magnetic nanoextraction, the surface of 1 mL MGNP was modified with a linker; 20 mM 0.1 mL mercaptoundecaonic acid (MUA) in ethanol. The mixture was incubated for 30 min and excess MUA was removed by washing with ethanol. Then, magnetic particles were re-suspended in 1 mL PBS, and carboxylate group of MUA on the surface of MGNP was activated using 0.2 mL EDC/NHS (0.1 M) for 30 min for antibody conjugation. After activation, they were incubated with 0.1 mL 100 μg/mL PVX-antibody at 4 °C for one night. Finally, they were washed with PBS for three times to remove free antibodies and they were re-suspended in 1 mL PBS.

PVX samples were prepared in PBS in different concentrations between 10 and 750 ppb. 50 μL of PVX-antibody modified MGNP were added to 100 μL PVX samples and the solutions were incubated for one hour at 4 °C. After three times washing with PBS, the sandwich assay procedure with DTNB labeled BAC-AuNR was applied: Firstly 100 μL 1% ethanolamine (*v*/v) were added to PVX captured MGNP

Table 1 Benzalkonium chloride optimization (100 μL seed, 1000 μL $HAuCl_4$ (1.86×10^{-3} M), 60 μL $AgNO_3$ (0.01 M), 250 μL ascorbic acid (0.1 M))

BAC concentration	Size (nm)	aspect ratio	Shape
1%	19.6 ± 4.6	1.3 ± 0.4	anisotropic spherical and cube
2%	22.4 ± 2.8	1.2 ± 0.1	anisotropic spherical and cube
4%	27.7 ± 8.7	1.5 ± 0.6	anisotropic spherical and cube
6%	32.4 ± 10	1.8 ± 0.6	anisotropic spherical and cube
8%	49.5 ± 6.1 × 25.9 ± 12	2.4 ± 1.3	rod
10%	45.5 ± 2.6 × 19.3 ± 5.1	2.5 ± 0.6	rod
11%	49.8 ± 4.4 × 18.2 ± 3.7	2.8 ± 0.4	rod
13%	45.6 ± 6.2 × 16.8 ± 4.0	2.8 ± 0.6	rod
14%	51.5 ± 8.1 × 26.6 ± 9.7	2.2 ± 0.7	rod
15%	39.4 ± 2.7 × 16.4 ± 2.2	2.4 ± 0.3	rod
20%	27.3 ± 5.9	1.4 ± 0.2	Anisotropic triangle, icosahedra and cube

The data reported as average sizes of 10 particles measured at TEM images. Sizes for rods were reported as longitudinal size x transverse size respectively

solutions and incubated for three hours to prevent non-specific interaction. Then 50 μL DTNB labeled and PVX antibody modified AuNR were added to the solutions. After one night incubation at 4 °C, particles were collected with a magnet and washed for three times. Finally, they were suspended in 100 μL PBS and 3 μL samples were dropped on aluminum foil covered glass slides for Raman measurement. Three replicates of PVX at 100, 300 and 500 ppb were prepared in PBS and analyzed according to above procedure for three days for analytical validation studies.

Results & discussion

It is well documented that the seed mediated growth procedure is the most practical method for the synthesis of AuNR. Generally, CTAB and gemini surfactants were used as shape – directing agents in seed mediated growth procedure. The resulting aspect ratio can be controlled by changing the concentration of $HAuCl_4$ and seed. In the present study, we describe the use of BAC as the directing agent for seed mediated growth of AuNR. BAC growth medium has some advantages over traditional CTAB based growth systems like BAC is less toxic and cheaper than CTAB. Although CTAB was used in seed synthesis and at later steps it was removed from particles so BAC is the primary surfactant for seeded growth of gold nanorods. The FTIR spectrum of BAC-AuNR shows that BAC exist on the surface of AuNR and CTAB which was used in seed synthesis was removed in seed mediated growth and washing procedures (Fig. S1–3). Although BAC and CTAB have similar molecular groups in their structures, it is possible to differentiate them in IR spectrum especially considering aromatic group of BAC and some other small differences in their spectra. Therefore, we employed FTIR spectroscopy to confirm only BAC exist on the surface of AuNR. Bands of BAC-AuNR mostly match with BAC while it differs more with CTAB. First and the most important IR absorption is at 1628 cm^{-1} assigned to partial double bonds of aromatic group in BAC and BAC-AuNR have also weaker form of that band. Also IR absorption at 3002 cm^{-1} is seen in BAC and BAC-AuNR spectra that is well known band for phenyl group which does not exist in CTAB FTIR spectrum. Asymmetric

Table 2 Gold concentration optimization (100 μL seed, 10% benzalkonium chloride, 60 μL $AgNO_3$, 250 μL ascorbic acid)

Gold concentration	Size (nm)	Aspect ratio	Shape
5.67×10^{-4} M	9.0 ± 1.1	1.1 ± 0.2	spherical
1.13×10^{-3} M	14.6 ± 1.4	1.0 ± 0.1	spherical
1.45×10^{-3} M	22.3 ± 2.5 × 11.6 ± 1.3	2.0 ± 0.4	elliptical rod
1.85×10^{-3} M	27.9 ± 4.6 × 10.9 ± 2.3	2.6 ± 0.5	elliptical rod
2.20×10^{-3} M	29.5 ± 3.6 × 14.8 ± 2.7	2.1 ± 0.5	elliptical rod

The data reported as average sizes of 10 particles measured at TEM images. Sizes for rods were reported as longitudinal size x transverse size respectively

Table 3 Seed volume optimization (1.85×10^{-3} M Au, % 10 benzalkonium chloride, 60 μL Ag, 250 μL ascorbic acid)

Seed volume	Size (nm)	Aspect ratio	Shape
50 μL	21 ± 3.0	1.5 ± 0.16	Spherical and rod
100 μL	30.8 ± 3.9 × 13.5 ± 1.9	2.2 ± 0.5	rod (dog-bone)
200 μL	17 ± 0.8	2.14 ± 0.22	spherical and rod
300 μL	21.5 ± 0.8 × 8.5 ± 0.9	3.6 ± 0.33	rod
400 μL	10.3 ± 0.7	3.1 ± 0.48	spherical and rod
600 μL	10.9 ± 0.8	1.72 ± 0.33	spherical and rod

The data reported as average sizes of 10 particles measured at TEM images. For mixtures, the data for the particle with higher fraction is reported. Sizes for rods were reported as longitudinal size x transverse size respectively

Table 4 Silver nitrate (0.01 M) volume optimization (1.85×10^{-3} M Au, % 10 benzalkonium chloride, 100 μL seed, 250 μL ascorbic acid

Seed volume	Size (nm)	Aspect ratio	Shape
15 μL	16.2 ± 2.1	1.1 ± 0.1	anisotropic spherical
30 μL	28.9 ± 2.9 × 14.2 ± 1.3	2.0 ± 0.3	rod
45 μL	25.0 ± 1.9 × 10.5 ± 1.0	2.4 ± 0.2	rod
60 μL	23.8 ± 3.0 × 10.0 ± 0.9	2.4 ± 0.5	rod
75 μL	23.4 ± 1.5 × 9.6 ± 0.5	2.4 ± 0.1	rod
100 μL	14.3 ± 0.5	2.5 ± 0.6	spherical and rod

The data reported as average sizes of 10 particles measured at TEM images. For mixtures, the data for the particle with higher fraction is reported. Sizes for rods were reported as longitudinal size x transverse size respectively

vibrations of CH_3–N^+ in BAC exactly match with BAC-AuNR 1457, 1467, 1476 cm^{-1} (ν_{asym} (CH_3–N^+)) while CTAB shows small differences having those peaks at 1462, 1473, 1486 cm^{-1}. The peaks at 1430, 1407 and 1396 cm^{-1} of CTAB are assigned to symmetric CH_3–N^+ vibrations and those vibrations can be seen at 1447 and 1378 for BAC and BAC-AuNR. Stretching of hydrocarbon chain (sp^3 C-H) around 2900 cm^{-1} also shows small differences between CTAB and BAC. This region of BAC-AuNR mostly matches with BAC while it is a little more different from CTAB. Finally, CTAB has strong bands at 912 and 961 cm^{-1} that do not exist in BAC-AuNR spectrum. While most of the bands of BAC can be clearly seen in BAC-AuNR, some bands were weaker in BAC-AuNR FTIR spectrum and it might be due to AuNR limits some vibrational and rotational modes of molecules attached on its surface. On the other hand, bands of CTAB do not coincide with BAC-AuNR bands. Consequently, FTIR spectrum of BAC-AuNR displays only BAC exist on the surface of AuNR. Therefore, as a surface protecting agent, BAC determines some characteristics of AuNR such as aggregation tendency, toxicity, etc.

Our approach to the formation of AuNR is to deposit Au^+ ions on the surface of gold seed in a fashion similar to seeded growth used in CTAB as a surface protecting agent. In this study, the surfactant solution used is BAC and the addition of gold chloride salt solution to a mixture of silver and BAC leads to the formation of a complex involving both benzalkonium ions (BA^+) and Au^{3+} which appeared as a pale – yellow. In consequence of reduction of Au^{3+} to Au^+ by ascorbic acid, Au^+ ions were deposited on to the small gold seeds in the presence of directing surfactant BAC and silver ions. The resulting aspect ratio can be controlled by changing the concentration of $HAuCl_4$, seed, BAC, silver and reducing agent.

Optimizations

The effect of BAC, $HAuCl_4$, seed, $AgNO_3$ and ascorbic acid concentration on gold nanoparticle size and shape were studied. In the first set of experiments, we investigated the effect of BAC concentration on aspect ratio. We observed remarkable changes in size and shape when the amount of BAC changed between 1 and 20% (Fig. S4). The change of shape in gold nanoparticles depending on BAC concentration could be originated from the fact that BAC might have different binding affinities to facets of gold nanoparticles. This may change the order of free energies for different planes and it can cause different growth rate in planes [31]. As a result, different shapes can be observed rather than spherical particles. We think that the increase of the amount of BAC can affect the difference of growth rate in planes resulting different particle shapes from spheres to rods. When BAC concentration increased from 1% to 6%, size of anistropic spheres and cubes increased from 20 nm to 40 nm (Table 1). After 8% BAC concentration, we observed rod formation. Anisotropic triangles, isocahedra and cubes were observed at 20% BAC

Table 5 Ascorbic acid (0.1 M) volume optimization (1.85×10^{-3} M Au, % 10 benzalkonium chloride, 100 μL seed, 60 μL Ag)

Ascorbic acid volume	Size (nm)	Aspect ratio	Shape
100 μL	19.7 ± 4.3	1.1 ± 0.1	anisotropic spherical
125 μL	26.8 ± 2.6 × 15.2 ± 4.1	1.8 ± 0.6	rod
150 μL	29.0 ± 4.1 × 9.2 ± 1.1	3.2 ± 0.7	rod
175 μL	31.5 ± 4.9 × 9.8 ± 0.5	3.2 ± 0.4	rod
200 μL	28.3 ± 2.4 × 9.6 ± 1.0	3.0 ± 0.2	rod
225 μL	23.6 ± 5.1 × 10 ± 0.1	2.4 ± 0.5	rod
250 μL	27.4 ± 3.7 × 11.3 ± 0.7	2.5 ± 0.3	rod

The data reported as average sizes of 10 particles measured at TEM images. Sizes for rods were reported as longitudinal size x transverse size respectively

concentration. Among these concentrations, 10% BAC concentration was selected for further studies due to higher yield, homogeneity, and repeatability.

We performed another set of experiment for gold concentration optimization keeping other parameters unaltered. The effect of gold concentration was investigated between 5.67×10^{-4} M – 2.20×10^{-3} M (Table 2). As expected, low gold concentrations yield spherical particles while rod-shaped particles were observed at higher concentrations of gold (Fig. S5). UV-Vis absorption spectra (Fig. S9) confirms TEM images by formation of a new band around 700 nm that belongs to longitudinal band on rod. The transverse band is around 530 nm. TEM image and a small shoulder of the transverse peak show that small amount of spherical particles still exists with rod shaped particles. Gold concentration was hold at 1.85×10^{-3} M for further optimization experiments.

Seed concentration also affected particle shape and sizes (Table 3). Seed volumes from 50 μL to 600 μL creates spherical, rod and mixture of these particles (Fig. S6). According to TEM images and UV-Vis absorption spectra (Fig. S10), we decided to use 100 μL seed for further experiments.

$AgNO_3$ amount, which was used to enhance yields in gold nanorod synthesis, was optimized between 15 and 100 μL (Table 4). After 30 μL of $AgNO_3$, rod formation was observed in TEM images (Fig. S7) with formation of a new UV-Vis absorption band (Fig. S11). 60 μL of $AgNO_3$ which yields more homogenous particle profile was selected as optimum amount.

Finally, we studied the effect of reducing agent, ascorbic acid in a range of 100–250 μL (Table 5). When 100 μL ascorbic acid was used, anisotropic spheres about 20 nm were observed. After 125 μL ascorbic acid, we observed rod formations with aspect ratio from 1.5 to 3 observed (Fig. S8 and Fig. S12). The final AuNR solution has blue color and zeta potential of 27.8 mV.

Optimized AuNR contain a little silver in it and silver content was found as 1.4 $\mu g \cdot mL^{-1}$ by ICP-MS measurements.

Modification with mercapto-compounds

After the synthesis, the surface of AuNR should be modified for intended application. For this purpose, the capping agent has to be replaced effectively with a new agent that has higher affinity to gold surfaces. We compared surface modification of CTAB-AuNR and BAC-AuNR with frequently used surface modifying agents, mercaptoundecanoic acid, lipoic acid and mercaptophenylboronic acid. According to S/Au ratio, BAC-AuNR has higher modification yield in mercaptoundecanoic acid modification while CTAB-AuNR show higher yields in lipoic acid and mercaptophenyl boronic acid modification according to ICP-MS measurements (Table S1). These results indicate that BAC-AuNR can be easily modified like CTAB-AuNR.

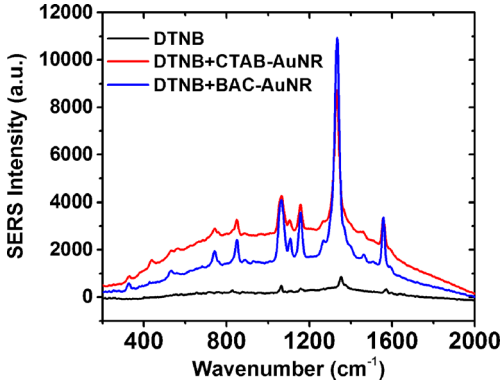

Fig. 1 Enhancements of DTNB Raman spectrum by CTAB-AuNR and BAC-AuNR

SERS applications of BAC-AuNR

Amplification of the Raman signals by metal nanostructures depends on hot spots created on sites of metal particles. These intensified electric fields that is responsible for surface enhanced light scattering effect depends on fabrication techniques of metal particles [26, 32]. Metal particles with different synthesis routes can have different signal enhancement effects in spectroscopy. We compared signal amplification of BAC-AuNR and CTAB-AuNR on a Raman dye, DTNB. SERS spectra (Fig. 1) show that BAC-AuNR has higher enhancement effect on DTNB than that of CTAB-AuNR. The calculated enhancement factor (EF) for BAC-AuNR is ~1.7×10^4 (see Electronic Supplementary Material for EF

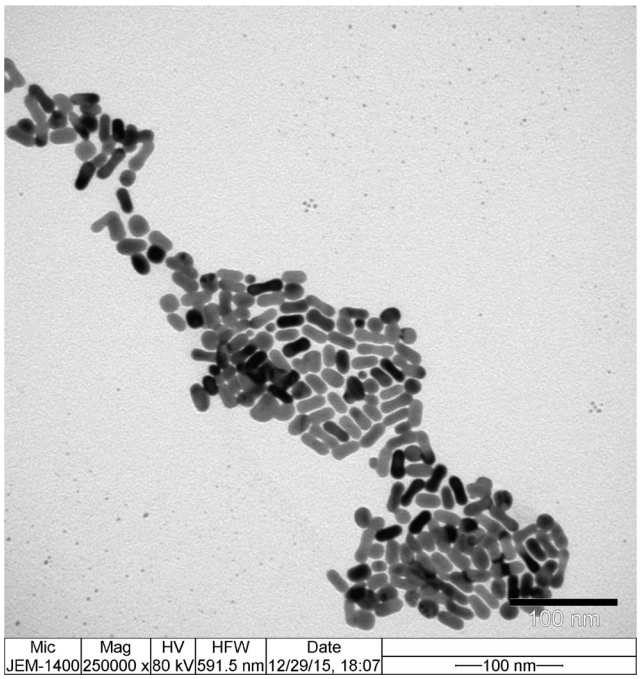

Fig. 2 TEM image of BAC-AuNR used in PVX determination

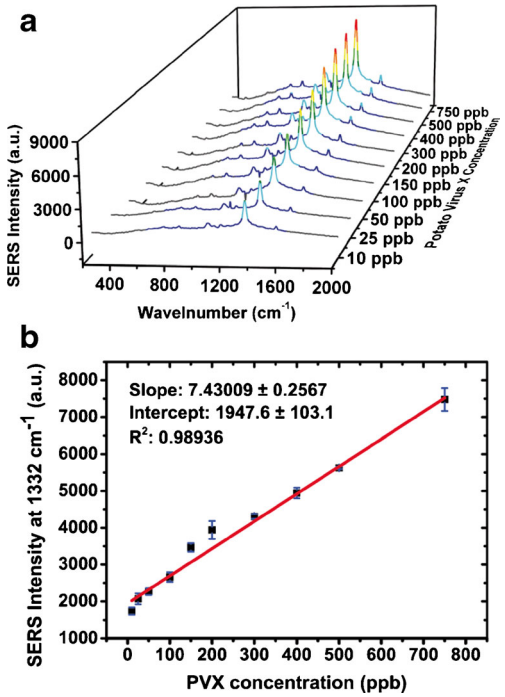

Fig. 3 SERS study of PVX determination based on Raman label (DTNB) measurements **a** calibration spectra **b** calibration graph

calculation). The results show that BAC-AuNR can be used for SERS analysis of samples which requires high sensitivity.

We also tested analytical performance of BAC-AuNR in a quantitative SERS analysis of a biologically important analyte, a virus. Fabrication of homogenous and stable nanostructures affects analytical parameters in quantitative SERS analysis because aggregated or heterogeneous particles have low repeatability and reproducibility in SERS. We tested the analytical performance of BAC-AuNR (Fig. 2) on PVX determination by sandwich assay with using raman labeled BAC-AuNR and MGNP. The strong peak at 1332 cm^{-1} in SERS spectra (Fig. 3a) were used in the quantitative analysis. Range was determined by observation of linear responses between PVX concentration and peak intensities. Linear relationship in the range of 10–750 ppb of PVX has high coefficient of determination in the calibration graph (Fig. 3b). Detection and quantitation limits were calculated as 2.2 ppb and 6.5 ppb respectively from slope and intercept values of calibration sets. Samples at three different concentration levels were analyzed to test accuracy and precision. High recoveries between 97.7–103.3% shows that the assay has high accuracy. Intra-day and inter-day precision were assessed by relative standard deviations of samples (Table S2). Validation results prove that BAC-AuNR can produce precise and accurate signals in SERS analysis.

Table 6 shows comparison of BAC-AuNR with some other SERS active particles in terms of application and enhancement factors. It is clear that the developed BAC-AuNR is not one of the best material in terms of enhancement factor but still it provides high-sensitivity comparing other detection techniques used in PVX detection such as UV absorbance in ELISA [33] since SERS itself is a high sensitive technique that even single molecule detection is possible with 10^7–10^8 enhancement factors. The enhancement factors of silver aggregates can reach to level of 10^{10} [34] however precision is generally low if they are used in quantitative analysis due to non-uniform structure of aggregates. In consequence, BAC-AuNR provides low toxicity, acceptable accuracy and precision for quantitative analysis and moderate sensitivity comparing other SERS active particles.

Conclusion

In this study, we developed a SERS active novel AuNR by using BAC as a stabilizing agent. BAC was used as a shape – directing agent in seed mediated growth procedure. The effects of chemicals-reducing agent, stabilizing agent, gold, and silver-were observed for homogenous and stable AuNR fabrication. TEM images indicated that the monodisperse AuNR were synthesized with a high yield. The high–yield

Table 6 Recent examples of SERS active nanomaterials

Material	Analyte	Matrices	Enhancement Factor	Reference
AgNP	Formaldehyde	Food samples and environmental waters	Not provided	[35]
AuNF	Dopamine		Not provided	[36]
AgNP	Pesticides	Food samples	1.2×10^8	[37]
Au-AgNR	Cervical cancer cells	Cell culture	Not provided	[38]
AuNP	Nicotine and uric acid		$\sim 10^7$	[39]
AuNR	Crystal violet and methylene blue		$\sim 10^4$	[40]
AuNR	4-nitrothiophenol		$\sim 10^7$	[41]
AuNR	Potato virus X		$\sim 1.7 \times 10^4$	this study

AgNP Silver nanoparticles, *AuNF* Gold nanoflowers, *Au-AgNR* Gold-silver nanorods

anisotropic growth and monodispersity of AuNR can be attributed to the use of BAC as a surfactant. Synthesized BAC-AuNR not only shows high signal amplification in Raman spectroscopy but also serves high analytical performance for quantitative analysis in SERS. High sensitivity was achieved in SERS measurements of DTNB. We also showed that the surface of BAC-AuNR can easily be modified with thiol containing compounds for different applications. Finally, we used BAC-AuNR in a quantitative SERS application for PVX determination. BAC can be a cheaper and safer alternative to CTAB in AuNR synthesis. This study concentrates on introduction of a new and less toxic surface protection agent in AuNR synthesis and exploring analytical performance of the AuNR in quantitative analysis. Further studies such as facet control study might be necessary to if higher enhancement factors desired.

Acknowledgements The authors acknowledge COST CA15114 - TUBITAK Project no: 114Z783 for the financial support.

Compliance with ethical standards The authors declare that they have no competing interest.

References

1. Schmid G (ed) (2010) Nanoparticles: from theory to application, 2nd edn. Wiley-Blackwell, Weinheim. doi:10.1002/9783527631544
2. Zhao P, Li N, Astruc D (2013) State of the art in gold nanoparticle synthesis. Coord Chem Rev 257(3–4):638–665. doi:10.1016/j.ccr.2012.09.002
3. Chen F, Wang Y, Ma J, Yang G (2014) A biocompatible synthesis of gold nanoparticles by Tris(hydroxymethyl)aminomethane. Nanoscale Res Lett 9:1–6. doi:10.1186/1556-276x-9-220
4. Dreaden EC, Alkilany AM, Huang X, Murphy CJ, El-Sayed MA (2012) The golden age: gold nanoparticles for biomedicine. Chem Soc Rev 41:2740–2779. doi:10.1039/c1cs15237h
5. Sperling RA, Rivera Gil P, Zhang F, Zanella M, Parak WJ (2008) Biological applications of gold nanoparticles. Chem Soc Rev 37(9):1896–1908. doi:10.1039/b712170a
6. Guerrero-Martínez A, Pérez-Juste J, Carbó-Argibay E, Tardajos G, Liz-Marzán LM (2009) Gemini-surfactant-directed self-assembly of monodisperse gold nanorods into standing Superlattices. Angew Chem Int Ed 48(50):9484–9488. doi:10.1002/anie.200904118
7. Perez-Juste J, Pastoriza-Santos I, Liz-Marzan LM, Mulvaney P (2005) Gold nanorods: synthesis, characterization and applications. Coord Chem Rev 249:1870–1901. doi:10.1016/j.ccr.2005.01.030
8. Zia R, Schuller JA, Chandran A, Brongersma ML (2006) Plasmonics: the next chip-scale technology. Mater Today (Oxford, U K) 9:20–27. doi:10.1016/s1369-7021(06)71572-3
9. Yu C, Varghese L, Irudayaraj J (2007) Surface modification of cetyltrimethylammonium bromide-capped gold nanorods to make molecular probes. Langmuir 23(17):9114–9119. doi:10.1021/la701111e
10. Ye X, Gao Y, Chen J, Reifsnyder DC, Zheng C, Murray CB (2013) Seeded growth of monodisperse gold nanorods using bromide-free surfactant mixtures. Nano Lett 13(5):2163–2171. doi:10.1021/nl400653s
11. Schacter D (2013) The source of toxicity in ctab and ctab-stabilized gold nanorods. Master of Science Thesis, The State University of New Jersey. doi:10.7282/T3X63KMS
12. Johnson CJ, Dujardin E, Davis SA, Murphy CJ, Mann S (2002) Growth and form of gold nanorods prepared by seed-mediated, surfactant-directed synthesis. J Mater Chem 12(6):1765–1770. doi:10.1039/b200953f
13. Liu G-SP (2005) Mechanism of silver(I)-assisted growth of gold nanorods and bipyramids. J Phys Chem B 109(47):22192–22200. doi:10.1021/jp054808n
14. Orendorff CJ, Murphy CJ (2006) Quantitation of metal content in the silver-assisted growth of gold nanorods. J Phys Chem B 110(9):3990–3994. doi:10.1021/jp0570972
15. Choi B-S, Iqbal M, Lee T, Kim YH, Tae G (2008) Removal of cetyltrimethylammonium bromide to enhance the biocompatibility of Au nanorods synthesized by a modified seed mediated growth process. J Nanosci Nanotechnol 8:4670–4674. doi:10.1166/jnn.2008.IC18
16. Connor EE, Mwamuka J, Gole A, Murphy CJ, Wyatt MD (2005) Gold nanoparticles are taken up by human cells but do not cause acute cytotoxicity. Small 1(3):325–327. doi:10.1002/smll.200400093
17. Koyama K, Shimazu Y (2005) Benzalkonium chlorides. Springer GmbH, pp 407–413. doi:10.1007/3-540-27579-7_45
18. Freeman PD, Kahook MY (2009) Preservatives in topical ophthalmic medications: historical and clinical perspectives. Expert Review of Ophthalmology 4(1):59–64. doi:10.1586/17469899.4.1.59
19. Pisella PJ, Fillacier K, Elena PP, Debbasch C, Baudouin C (2000) Comparison of the effects of preserved and unpreserved formulations of Timolol on the ocular surface of albino rabbits. Ophthalmic Res 32(1):3–8
20. Törnblom M, Henriksson U (1997) Effect of Solubilization of aliphatic hydrocarbons on size and shape of Rodlike C16TABr micelles studied by 2H NMR relaxation. J Phys Chem B 101(31):6028–6035. doi:10.1021/jp970899f
21. Zhu Y, Free ML (2015) Evaluation of ion effects on surfactant aggregation from improved molecular thermodynamic modeling. Ind Eng Chem Res 54:9052–9056. doi:10.1021/acs.iecr.5b02103
22. Grzelczak M, Perez-Juste J, Mulvaney P, Liz-Marzan LM (2008) Shape control in gold nanoparticle synthesis. Chem Soc Rev 37(9):1783–1791. doi:10.1039/b711490g
23. Schluecker S (2011) SERS microscopy: nanoparticle probes and biomedical applications. In: Wiley-VCH Verlag GmbH & Co. KGaA, pp 263–283. doi:10.1002/9783527632756.ch12
24. Wang Y, Wang E (2010) Nanoparticle SERS substrates. In: Surface enhanced Raman spectroscopy. Wiley-VCH Verlag GmbH & Co. KGaA, pp 39–69. doi:10.1002/9783527632756.ch2
25. Yang Y, Liu J, Fu Z-W, Qin D (2014) Galvanic replacement-free deposition of Au on Ag for Core–Shell Nanocubes with enhanced chemical stability and SERS activity. J Am Chem Soc 136(23):8153–8156. doi:10.1021/ja502472x
26. Rycenga M, Xia X, Moran CH, Zhou F, Qin D, Li Z-Y, Xia Y (2011) Generation of hot spots with silver Nanocubes for single-molecule detection by surface-enhanced Raman scattering. Angew Chem Int Ed 50(24):5473–5477. doi:10.1002/anie.201101632
27. Guven B, Basaran-Akgul N, Temur E, Tamer U, Boyac IH (2011) SERS-based sandwich immunoassay using antibody coated magnetic nanoparticles for *Escherichia coli* enumeration. Analyst 136(4):740–748. doi:10.1039/c0an00473a
28. Ulman A (1996) Formation and structure of self-assembled monolayers. Chem Rev (Washington, DC) 96:1533–1554. doi:10.1021/cr9502357
29. Batten JS, Yoshinari S, Hemenway C (2003) Potato virus X: a model system for virus replication, movement and gene expression.

Mol Plant Pathol 4(2):125–131. doi:10.1046/j.1364-3703.2003.00156.x
30. Tamer U, Guendogdu Y, Boyaci IH, Pekmez K (2010) Synthesis of magnetic core-shell Fe3O4-Au nanoparticle for biomolecule immobilization and detection. J Nanopart Res 12:1187–1196. doi:10.1007/s11051-009-9749-0
31. Xia Y, Xiong Y, Lim B, Skrabalak SE (2009) Shape-controlled synthesis of metal nanocrystals: simple chemistry meets complex physics? Angew Chem Int Ed 48(1):60–103. doi:10.1002/anie.200802248
32. Alonso-González P, Albella P, Schnell M, Chen J, Huth F, García-Etxarri A, Casanova F, Golmar F, Arzubiaga L, Hueso LE, Aizpurua J, Hillenbrand R (2012) Resolving the electromagnetic mechanism of surface-enhanced light scattering at single hot spots. Nat Commun 3:684. doi:10.1038/ncomms1674l
33. Weilbach A, Sander E (2000) Quantitative detection of potato viruses X and Y (PVX, PVY) with antibodies raised in chicken egg yolk (IgY) by ELISA variants. Journal of Plant Diseases and Protection 107(3):318–328
34. Le Ru EC, Blackie E, Meyer M, Etchegoin PG (2007) Surface enhanced Raman scattering enhancement factors: a comprehensive study. J Phys Chem C 111(37):13794–13803. doi:10.1021/jp0687908
35. Ma P, Liang F, Wang D, Yang Q, Ding Y, Yu Y, Gao D, Song D, Wang X (2015) Ultrasensitive determination of formaldehyde in environmental waters and food samples after derivatization and using silver nanoparticle assisted SERS. Microchim Acta 182(3):863–869. doi:10.1007/s00604-014-1400-9
36. Bu Y, Lee SW (2015) Flower-like gold nanostructures electrodeposited on indium tin oxide (ITO) glass as a SERS-active substrate for sensing dopamine. Microchim Acta 182(7):1313–1321. doi:10.1007/s00604-015-1453-4
37. Pan Y, Guo X, Zhu J, Wang X, Zhang H, Kang Y, Wu T, Du Y (2015) A new SERS substrate based on silver nanoparticle functionalized polymethacrylate monoliths in a capillary, and it application to the trace determination of pesticides. Microchim Acta 182(9):1775–1782. doi:10.1007/s00604-015-1514-8
38. Bamrungsap S, Treetong A, Apiwat C, Wuttikhun T, Dharakul T (2016) SERS-fluorescence dual mode nanotags for cervical cancer detection using aptamers conjugated to gold-silver nanorods. Microchim Acta 183(1):249–256. doi:10.1007/s00604-015-1639-9
39. Villa JEL, Santos DP, Poppi RJ (2016) Fabrication of gold nanoparticle-coated paper and its use as a sensitive substrate for quantitative SERS analysis. Microchim Acta 183(10):2745–2752. doi:10.1007/s00604-016-1918-0
40. Vassalini I, Rotunno E, Lazzarini L, Alessandri I (2015) "Stainless" gold nanorods: preserving shape, optical properties, and SERS activity in oxidative environment. ACS Appl Mater Interfaces 7(33):18794–18802. doi:10.1021/acsami.5b07175
41. Zhang Q, Han L, Jing H, Blom DA, Lin Y, Xin HL, Wang H (2016) Facet control of gold nanorods. ACS Nano 10(2):2960–2974. doi:10.1021/acsnano.6b00258